Applied Physics B (2025) 131:232
https://doi.org/10.1007/s00340-025-08579-9

Applied Physics B
Lasers and Optics

RESEARCH

Passively Q-switched high-repetition-rate Yb:LuGG channel waveguide laser

Deok Woo Kim[1] · Seong-Eun Lim[1] · Ji-Hoon Park[1] · Xavier Mateos[2] · Weidong Chen[3] · Carolina Romero[4,5] · Javier Rodríguez Vázquez de Aldana[4,5] · Fabian Rotermund[1]

Received: 13 August 2025 / Accepted: 9 October 2025 / Published online: 17 November 2025

Abstract

We report on a compact, passively Q-switched waveguide laser fabricated via femtosecond direct laser writing (fs-DLW) in an Yb:LuGG crystal. Prior to Q-switching experiments, continuous-wave operation was systematically characterized under various cavity configurations, achieving a maximum output power of 678 mW and a slope efficiency of 53.6% using a 70% output coupler. Passive Q-switching was implemented by incorporating single-walled carbon nanotubes (SWCNTs) as a saturable absorber, enabling stable laser operation over several hours. The 7.39-mm-long waveguide laser operated near 1030 nm, and its Q-switched performance was investigated using three output couplers with different transmissions. The best performance was obtained with a 50% output coupler, yielding pulses as short as 35 ns, a maximum output power of 478 mW, and a highest repetition rate of 2.51 MHz. These results demonstrate the excellent compatibility between fs-DLW-fabricated Yb:LuGG waveguides and SWCNT-based saturable absorbers, offering a promising route toward robust and highly efficient compact pulsed laser sources.

1 Introduction

The growing demand for compact, high-repetition-rate pulsed lasers operating at hundreds of kHz or higher has driven rapid advancements in laser miniaturization across various platforms. These developments are motivated by applications in scientific research, industrial processing, military systems, and medical technologies [1–7]. Among the diverse laser architectures, waveguide (WG) lasers have emerged as particularly promising candidates for integrated coherent light sources, offering strong potential for efficient chip-scale implementation [8–13].

Among the available WG fabrication techniques, femtosecond direct laser writing (fs-DLW) in crystalline materials enables the formation of channel WGs with highly uniform cross-sections along the propagation axis. This structural uniformity minimizes beam divergence and ensures excellent spatial mode overlap with the pump beam. As a result, fs-DLW WGs exhibit lower lasing thresholds and higher efficiency [14, 15].

In terms of host materials, gallium garnet crystals with the chemical formula $RE_3Ga_5O_{12}$ (RE = Gd, Y, Lu, abbreviated as REGG) are highly attractive due to their optical quality and thermal conductivity. Notably, in contrast to $Y_3Al_5O_{12}$ (YAG), these materials exhibit only a minimal reduction in thermal conductivity even at high levels of active-ion doping, enabling robust laser operation under demanding conditions [16–21]. Among the REGG family, Lu-based hosts have received particular attention. The close match in ionic radii and atomic mass between Yb^{3+} and Lu^{3+} ions minimizes lattice distortion, enhances crystal uniformity, and allows high doping concentrations without compromising optical quality [22–24]. Therefore, the synergistic combination of the favorable crystalline properties

✉ Fabian Rotermund
rotermund@kaist.ac.kr

1 Department of Physics, Korea Advanced Institute of Science and Technology (KAIST), Daejeon 34141, Republic of Korea

2 Física i Cristal·lografia de Materials (FiCMA), Universitat Rovira I Virgili (URV), 43007 Tarragona, Spain

3 State Key Laboratory of Functional Crystals and Devices, Fujian Institute of Research On the Structure of Matter, Chinese Academy of Sciences, Fuzhou 350002, China

4 Grupo de Investigación en Aplicaciones del Láser y Fotónica, University of Salamanca, 37008 Salamanca, Spain

5 Unidad de Excelencia en Luz y Materia Estructuradas (LUMES), Universidad de Salamanca, 37008 Salamanca, Spain

of LuGG and the intrinsic advantages of Yb^{3+}, including the absence of deleterious energy-transfer processes and a low quantum defect due to the close match between pump and laser wavelengths [25], makes Yb:REGG crystals highly promising candidates for compact and stable lasers across a broad range of operational regimes. Despite these advantages, fs-DLW-fabricated Yb:LuGG WG lasers have not yet been experimentally demonstrated.

In recent years, low-dimensional nanomaterials such as topological insulators, transition metal dichalcogenides, and carbon-based nanostructures have attracted significant attention as saturable absorbers (SAs) in passively pulsed lasers [26–32]. Among them, SWCNTs are particularly appealing due to their broadband linear and nonlinear absorption, ultrafast response times, straightforward fabrication, and ease of integration into optical devices. These characteristics not only facilitate laser miniaturization but also support diverse interaction schemes between the laser field and the SA [8, 9, 33–37]. In combination with the minimal beam divergence inherent to fs-DLW WGs, SWCNTs enable the realization of nearly-monolithic laser configurations with simplified designs, serving as viable alternatives to bulky active Q-switching elements.

In this work, we report for the first time the passively Q-switched operation in a fs-DLW-fabricated Yb:LuGG channel WG laser using SWCNTs as the SA. The experimental procedure involved a stepwise cavity configuration, beginning with bare-crystal lasing, followed by integration of a high-reflective mirror, and culminating in the full cavity assembly for both CW and Q-switched operation. Under CW operation, a maximum output power of 678 mW with a slope efficiency of 53.6% was achieved using a 70% output coupler (OC). Stable pulsed operation was subsequently realized by attaching a high-reflective mirror and a SWCNT-coated OC to the input and output facets of the WG, respectively, yielding stable performance over several hours. Q-switched operation was investigated using OCs with transmissions of 1%, 10%, and 50%. Pulse trains were obtained with repetition rates of 1.22 MHz, 1.61 MHz, and 2.51 MHz, and corresponding pulse durations of 72 ns, 49 ns, and 35 ns. At maximum pump power, the average output powers were 22 mW, 187 mW, and 478 mW, respectively.

2 Fabrication of waveguides and SWCNT-SA

The gain medium used in this experiment was a 7.39-mm-long Yb:LuGG with 10 at.% Yb^{3+} ion doping concentration. WG fabrication was performed using a Ti:sapphire amplifier system delivering ultrashort pulses centered at 800 nm with a pulse duration of ~ 60 fs at a repetition rate of 5 kHz [15]. The pulse energy incident on the crystal surface was precisely controlled to ~ 55 nJ by employing a combination of neutral density filters, half-wave plates, and a polarizer. These pulses were tightly focused into the Yb:LuGG crystal using a 40 × microscope objective lens. Permanent refractive index modifications were induced by translating the crystal at a constant speed of 600 μm/s, resulting in the formation of laser-inscribed damage tracks. The resulting WG featured a circular, unmodified core with a diameter of approximately 40 μm, surrounded by laser-induced damage regions that served as a depressed cladding.

For the transmission-type SA deposited on the appropriate output coupler, we used arc-discharged SWCNT powder (NanoIntegris Technologies, Inc.), which exhibits a broadband linear absorption in the 1-μm wavelength range [38]. The SWCNT powder was dispersed in 1,2-dichlorobenzene (o-DCB) at a concentration of 0.5 mg/mL. The dispersion underwent ultrasonification for 6 h, followed by centrifugation for 30 min. The supernatant containing well-dispersed SWCNTs was collected and mixed in equal volume with a PMMA solution (100 mg/mL in o-DCB, Polymer Source, Inc.). The resulting composite was then uniformly spin-coated onto selected output couplers. The linear and nonlinear optical properties of the SWCNT-SA used in this work are comparable to those reported in previous studies [12].

3 Experimental setup for compact Q-switching

Figure 1 illustrates the systematic experimental approach used to characterize the compact WG laser through across three sequential configurations. The pump source was a tapered amplified diode laser (TA pro, Toptica Photonics Inc.) operating at 970 nm, capable of delivering up to ~ 1.7-W output power before reaching the focusing lens (FL). The center wavelength of the pump beam was finely tuned to optimize absorption in the Yb:LuGG crystal. To precisely control both the pump power and polarization state, two half-wave plates and a polarizer were inserted along the beam path prior to the FL, ensuring a p-polarized pump beam. The beam was focused onto the WG end facet using an FL with a focal length of 35 mm. The pump beam waists at the focal point in the x and y directions were measured to be 14 μm and 15 μm, respectively, with corresponding M^2 factors of 1.36 and 1.30. The experimental investigation was conducted in three distinct stages as depicted in Fig. 1a, b and c. In the first configuration, CW lasing was evaluated using a bare WG crystal without any mirrors, see Fig. 1a. In the second step, a high-reflective (HR) mirror was added to the input facet of the WG to reflect the laser beam initially propagating along the pump direction back toward the

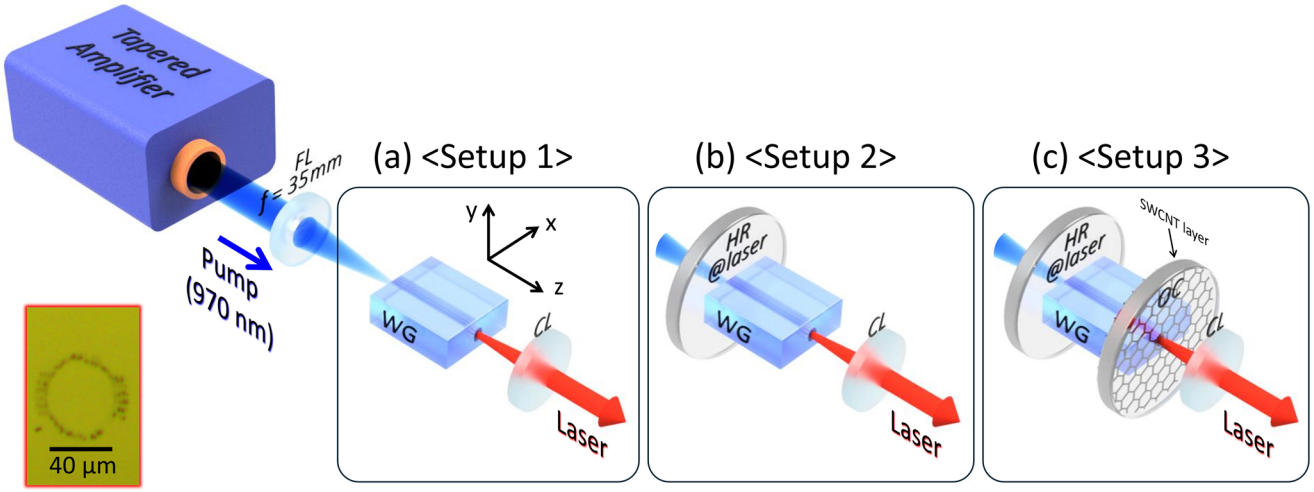

Fig. 1 Experimental setups used for the characterization of the compact WG laser. **a** Bare WG crystal without any mirror, **b** configuration with a HR mirror as the input coupler, and **c** complete laser cavity configuration with an OC for both CW operation (without SWCNT layer) and Q-switched operation (with SWCNT layer). *FL* pump beam focusing lens; *HR* high-reflective mirror at the laser wavelength; *WG* Yb:LuGG WG, *OC* output coupler; *CL* collimation lens. The inset (red-box) shows an optical microscope image of the WG facet

detection side, see Fig. 1b. Finally, in the third configuration, an OC was precisely aligned and attached to the output facet of the WG, forming a compact, fully assembled laser cavity, see Fig. 1c. In this final configuration, two operational regimes were investigated using the same cavity. CW operation was characterized using a pristine OC without any SAs. Subsequently, a SWCNT layer was spin-coated onto the face of the OC contacting the WG facet to achieve Q-switching, enabling a direct comparison between CW and Q-switched operation under identical cavity conditions. The laser output from the WG was collimated using a lens with a 40-mm focal length and passed through a long-pass filter with high transmission (>99%) at the laser wavelength to eliminate residual pump radiation.

4 Results on laser operation

4.1 CW operation characteristics

Before investigating Q-switched operation, we systematically characterized the CW performance of the WG laser under different cavity configurations and OC transmissions. The incident pump power was estimated by accounting for losses introduced by the focusing lens (FL), the HR mirror, and Fresnel reflections at the normally incident WG facet. Due to the inherently high gain properties of the Yb:LuGG crystal and the structural advantages of the fabricated WG, lasing could be achieved solely via Fresnel reflections from both crystal end facets when the pump beam was focused into the WG. Furthermore, assuming that gallium garnet crystals have similar refractive index dispersion, the Fresnel reflectance at the WG facet was estimated to be 10% [39], and the T_{OC} in this configuration is 99%. In this cavity setup, a laser beam counter-propagating to the pump beam's incident direction is also emitted, however, the measured laser output corresponds only to the direction toward the detection side. No damage to the pump source from the backward-propagating laser beam was observed, owing to the embedded optical isolator in the pump system and the long optical path between the pump source output aperture and the WG.

Figure 2a presents the input-output characteristics in the absence of a dedicated OC. Without the HR mirror, lasing was achieved with a maximum output power of 315 mW and a slope efficiency (η) of 34.6%. When a HR mirror was attached to one end of the WG, cavity losses were reduced and the counter-propagating laser beam initially directed along the pump beam axis, was reflected back toward the detection side. This modification decreased the lasing threshold (P_{th}) from 597 to 370 mW and simultaneously increased the output power. With the HR mirror in place, the maximum output power and slope efficiency increased to 629 mW and 56.5%, respectively. The inset in Fig. 2a shows a representative far-field mode profile confirming single-transverse-mode operation without high-order modes. The corresponding laser spectra for both configurations are shown in Fig. 2b, measured using an optical spectrum analyzer (86142A, Agilent) with a resolution bandwidth (RBW) of 0.06 nm. The laser spectrum obtained from the bare WG crystal (without any mirror) was centered around 1025 nm and exhibited periodic modulations with a mode spacing of ~0.2 nm. These multiple longitudinal spectral modes could be completely suppressed by attaching an HR mirror,

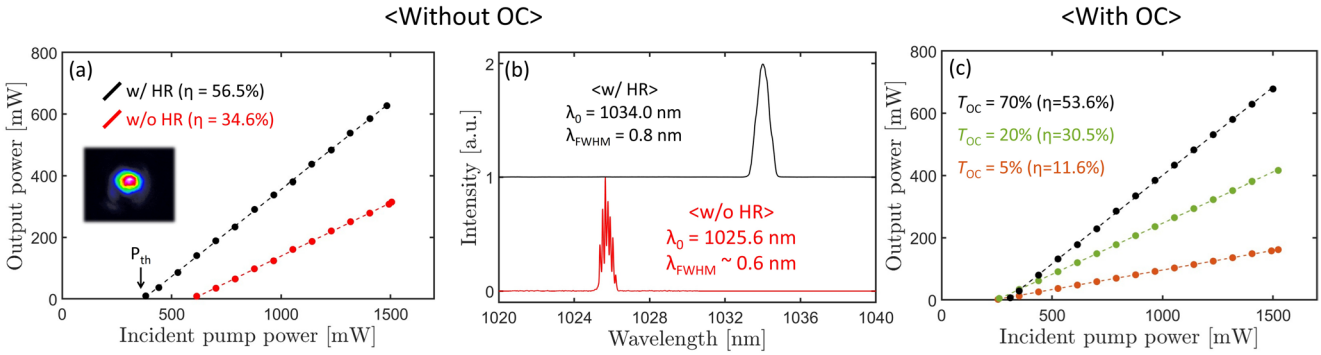

Fig. 2 CW operation characteristics. **a** Input–output power characteristics for configurations with (black) and without (red) HR mirror. The inset shows the far-field mode profile obtained with HR mirror. **b** Comparison of laser spectra for the configurations without (red) and with (black) HR mirror (black). **c** Input–output power characteristics for different OC transmissions: 5%, 20%, and 70%. The corresponding T_{OC} and slope efficiencies are indicated using the same color scheme as the respective plots

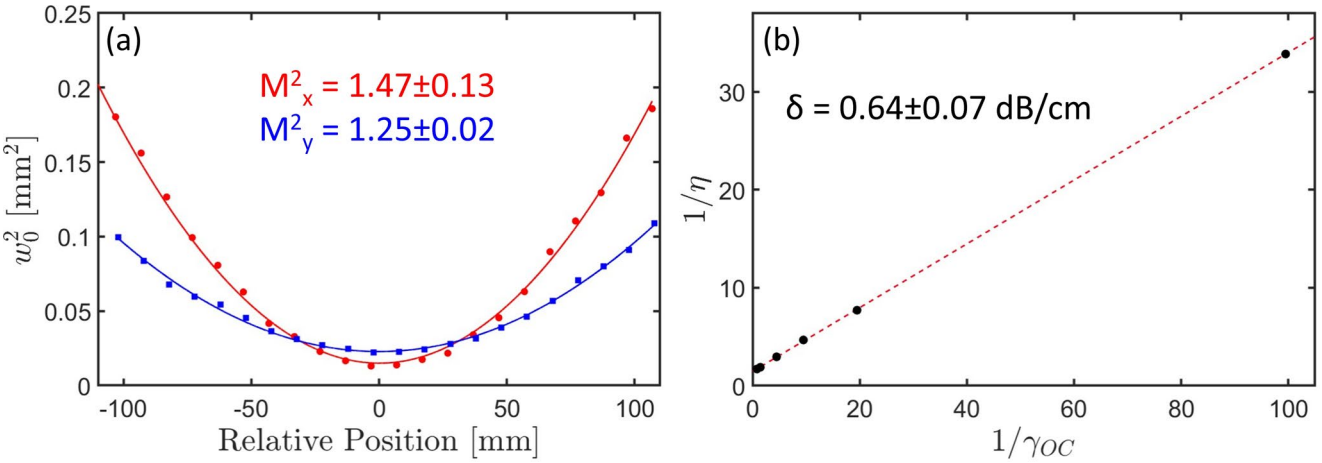

Fig. 3 **a** Knife-edge measurement traces, used to evaluate the beam propagation factor (M^2) of the laser beam along the x (red) and y (blue) axes. **b** Caird analysis plot (black circles) with linear fitting (red dashed line), showing the inverse of slope efficiency ($1/\eta$) as a function of inverse of output-coupling loss ($1/\gamma_{OC}$)

which shifted the central lasing wavelength to ~1034 nm due to the decrease in T_{OC} from 99 to 90%, resulting from the enhanced feedback. This spectral redshift with reduced cavity loss is a typical phenomenon attributed to the quasi-three-level nature of the Yb-ion. Subsequently, detailed input-output characterizations were performed for various OC transmissions (T_{OCs}) ranging from 1 to 70%. Figure 2c presents representative results for T_{OC} values of 5%, 20%, and 70%, while additional results for T_{OCs} of 1%, 10%, and 50% are shown separately in Fig. 4. As T_{OC} increased, both the maximum output power and slope efficiency improved. Specifically, for T_{OC} of 5%, 20%, and 70%, the maximum output powers reached 162 mW, 416 mW, and 678 mW, with corresponding slope efficiencies of 11.6%, 30.5%, and 53.6%, respectively. The lasing thresholds under these conditions were 234 mW, 249 mW, and 295 mW, respectively. In addition, the small-signal absorption under non-lasing conditions was measured to be >99.5%. Under lasing conditions, although a slight decrease of approximately 1% in pump absorption was observed due to weak ground-state bleaching, a pump absorption of exceeding 99.2% was maintained in all lasing configurations with an OC, owing to the high reflectance of the OC at the pump wavelength (ranging from 98 to 32% for T_{OCs} of 1–70%).

The diffraction characteristics of the laser beam in the Fig. 1b configuration were evaluated, and the results are shown in Fig. 3a. The M^2 factors in the x and y directions were determined to be 1.47±0.13 and 1.25±0.02, respectively. Based on both the far-field beam profile and these measurements, it is confirmed that the laser beam emitted from the WG exhibits propagation characteristics close to the diffraction limit. Furthermore, Caird analysis was performed using the T_{OC} values and the measured slope efficiencies, yielding a single-pass cavity loss (δ) of 0.64±0.07 dB/cm [40], as shown in Fig. 3b.

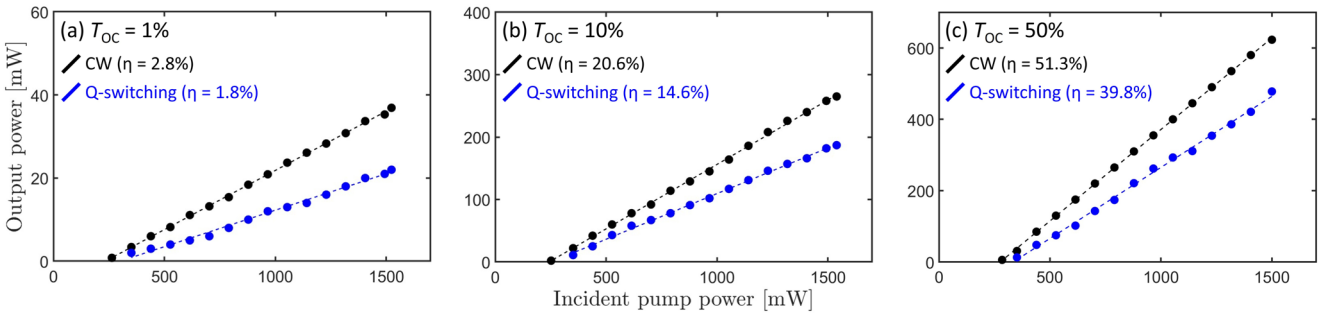

Fig. 4 Input–output power characteristics for CW (black) and Q-switched (blue) operation at T_{OC} of **a** 1%, **b** 10%, and **c** 50%. The corresponding slope efficiencies for each operating regime are indicated in the plots

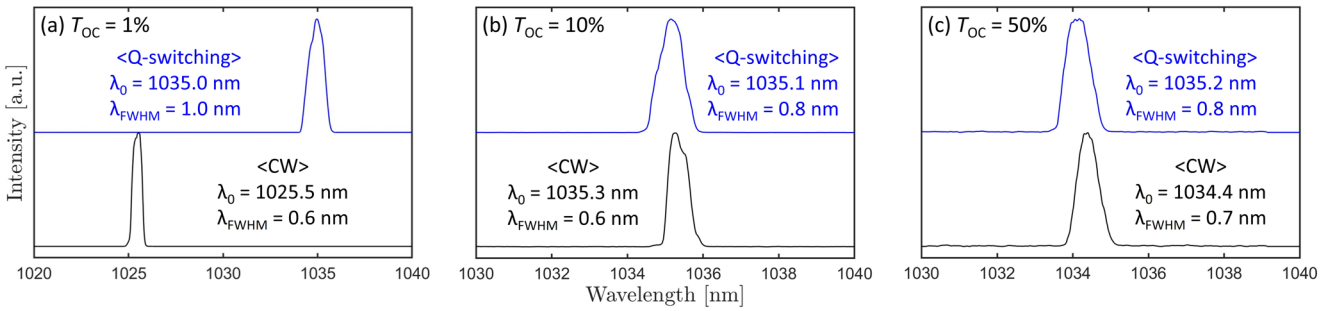

Fig. 5 Optical spectra of the laser output under CW (black) and Q-switched (blue) operations for OCs with transmissions of **a** 1%, **b** 10%, and **c** 50%

4.2 Output power characteristics in Q-switched operation

In the Q-switched laser experiments, three different OCs with transmissions of 1%, 10%, and 50% were employed. Figure 4 shows the input–output power characteristics for both CW and Q-switched operation. For T_{OC} = 1%, the slope efficiency and maximum output power (P_{max}) decreased slightly from 2.8% and 37 mW under CW operation to 1.8% and 22 mW under Q-switched operation, see Fig. 4a. By varying the pump power, the pulse energy could be tuned from 4.2 to 18 nJ, corresponding to peak powers ranging from 8.8 mW to 0.25 W. Similarly, for T_{OC} = 10%, the slope efficiency and P_{max} decreased from 20.6% and 265 mW (CW) to 14.6% and 187 mW (Q-switched) upon introducing the SWCNT-coated OC, see Fig. 4b. In this regime, the pulse energy was tunable from 13 to 116 nJ, with corresponding peak powers ranging from 0.12 to 2.37 W. The highest output performance was achieved with T_{OC} = 50%, yielding slope efficiencies and maximum output powers of 51.3% and 623 mW in CW operation, and 39.8% and 478 mW under Q-switched operation, respectively, see Fig. 4c. This configuration also provided the widest range of pulse energies, from 15 to 190 nJ, and peak powers from 0.08 to 5.43 W. The corresponding pulse repetition rates and durations as functions of pump power for all OCs are presented in Fig. 6, demonstrating clear tunability of the temporal characteristics across the full T_{OC} range.

4.3 Spectral characteristics in CW and Q-switched operations

Figure 5 shows the output spectra recorded at the maximum incident pump power for three different OCs under both CW and Q-switched regimes. For T_{OC} = 1%, the CW emission was centered at 1025.5 nm (λ_0), which redshifted to 1035.0 nm under Q-switched regime, Fig. 5a. Concurrently, the spectral bandwidth (λ_{FWHM}) increased from 0.6 to 1.0 nm. At higher T_{OC}, the center wavelength remained near 1035 nm, while a similar trend of spectral broadening was observed when transitioning from CW to Q-switched operation, see Fig. 5b and c. Specifically, for T_{OC} = 10%, both CW and Q-switched emission were centered at around 1035 nm with the bandwidth increasing from 0.6 to 0.8 nm. For T_{OC} = 50%, the shift tendency of the center wavelength and bandwidth broadening were also observed. Across all investigated conditions, the spectra exhibited clean, well-defined profiles with negligible spectral modulation, confirming stable and consistent laser performance throughout the full range of OC transmissions.

4.4 Q-switching tendency depending on pump power

The temporal dynamics of passively Q-switched lasers as a function of pump power can be qualitatively understood using laser rate equations [41]. For a given set of cavity components, as the pump power increases, the intracavity intensity rises, leading to faster bleaching of the SA. This accelerates the onset of lasing, resulting in shorter pulse duration. Simultaneously, the gain medium recovers more rapidly at higher pump power levels, reducing the time required to accumulate sufficient population inversion for the next pulse. As a result, the pulse repetition rate increases with increasing pump power. Furthermore, the combination of the inherently high emission cross-section of the Yb:LuGG crystal, the high-efficiency gain provided by the WG structure, and the low modulation depth of SWCNTs enabled Q-switching at MHz-level repetition rates. The short, mm-scale cavity length further reduced the round-trip time to approximately 100 ps, allowing the generation of ns-level short pulses.

The temporal pulse sequences were recorded using a fast InGaAs photodiode (ET-3500, Electro-Optic Technology Inc.) and a high-bandwidth oscilloscope (DPO71254, Tektronix) with bandwidths of 2 GHz and 12.5 GHz, respectively. To analyze the frequency components of the repetitive Q-switched pulses, a radio-frequency (RF) spectrum analyzer (E4407B, Agilent) with a RBW of 10 kHz was employed. The RF spectral measurement (inset in Fig. 6) confirms stable Q-switched operation, exhibiting well-defined fundamental frequencies and harmonic beat notes across the entire pump power range, indicating robust and consistent temporal stability.

Figure 6 presents the pump-dependent dynamics and frequency characteristics of the Q-switched pulse trains. Several key trends are observed: as the pump power increases, the pulse duration decreases, while the repetition frequency increases—behaviors typical of passively Q-switched lasers. This reflects efficient energy extraction and effective nonlinear modulation. Oscilloscope traces in Fig. 6a, d and g display stable and periodic pulse trains over a 50 μs time span at different incident pump powers. As the pump power increases, the repetition rates increase and the interpulse interval decreases. At the maximum available pump power (~1.5 W), the highest repetition rates achieved were 1.22 MHz, 1.61 MHz, and 2.51 MHz for T_{OC} = 1%, 10%, and 50%, respectively. The corresponding expanded views of individual pulses reveal clean, nearly symmetric profiles with negligible modulation or instability, as seen in Fig. 6b, e, and h. The shortest pulse durations (τ_{QS}) are 72 ns, 49 ns, and 35 ns for the same respective OCs. The corresponding RF spectra, recorded over 15 MHz span and shown in insets in Fig. 6b, e and h, exhibit strong fundamental and harmonic frequency components without any modulation sidebands, further confirming the stability of the Q-switched regime across the entire pump power range for all OCs. Figure 6c, f and i summarize the pulse duration and repetition frequency as functions of pump power, with parameters extracted directly from the oscilloscope traces. For T_{OC} = 1%, 10%, and 50%, the pulse duration and repetition rate can be tuned from 480 to 72 ns and 0.33 MHz to 1.22 MHz, from 111 to 49 ns and 0.84 MHz to 1.61 MHz, and from 195 to 35 ns and 0.89 MHz to 2.51 MHz, respectively. While the repetition rate for a given cavity configuration is primarily determined by the pump power, the choice of the OC sets the maximum achievable repetition rate for that configuration. A notable feature of this laser is the increase in the maximum achievable repetition rate with higher T_{OC}. This behavior is attributed to the increased intracavity losses associated with larger T_{OC}, which elevate the relaxation oscillation frequency and thereby favor higher repetition rate Q-switching dynamics. The representative laser performance parameters under both CW and Q-switched operation at maximum pump power are summarized in Table 1.

Fig. 6 Temporal and RF spectral characteristics of Q-switched operation. The top **a**–**c**, middle **d**–**f**, and bottom **g**–**i**) rows correspond to T_{OC} = 1%, 10%, and 50%, respectively. **a**, **d**, **g** Oscilloscope traces of pulse trains recorded over a 50 μs time span at various incident pump powers. **b**, **e**, **h** Expanded views of individual pulses with corresponding RF spectra shown in the insets. **c**, **f**, **i** Q-switching performance: pulse durations and repetition rates plotted as functions of incident pump power

The results presented here demonstrate the potential of the Yb:LuGG WG platform for robust, high-repetition-rate pulsed operation. Further advancements toward GHz-level repetition rates, typically achieved via passive mode-locking, could be envisioned in this quasi-monolithic cavity configuration. Achieving this would require several modifications to the current laser design. Employing smaller-core WGs would significantly increase the intracavity intensity, which is essential for reducing the critical pulse energy and enhancing nonlinear effects, such as self-phase modulation, to initiate mode-locking. Additionally, stable mode-locking in this high-repetition-rate regime would require increased pump power to provide sufficient intracavity laser power and appropriate dispersion management–precisely balancing group delay dispersion and self-phase modulation using suitable chirped mirrors–to support stable soliton pulse formation.

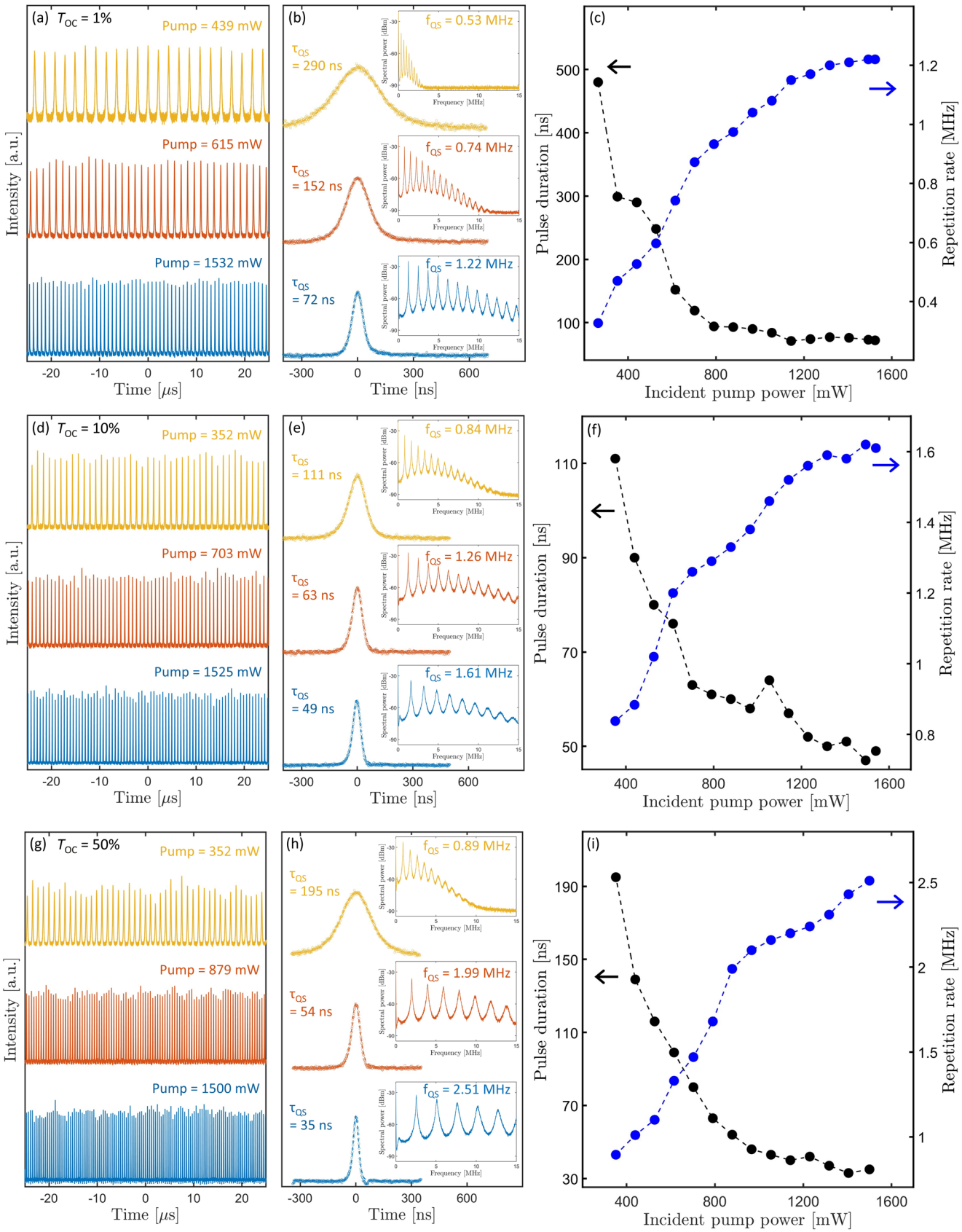
(a) T_{OC} = 1%
Pump = 439 mW
Pump = 615 mW
Pump = 1532 mW
Intensity [a.u.]
Time [μs]
(b)
τ_{QS} = 290 ns
f_{QS} = 0.53 MHz
τ_{QS} = 152 ns
f_{QS} = 0.74 MHz
τ_{QS} = 72 ns
f_{QS} = 1.22 MHz
Spectral power [dBm]
Frequency [MHz]
Time [ns]
(c)
Pulse duration [ns]
Repetition rate [MHz]
Incident pump power [mW]
(d) T_{OC} = 10%
Pump = 352 mW
Pump = 703 mW
Pump = 1525 mW
(e)
τ_{QS} = 111 ns
f_{QS} = 0.84 MHz
τ_{QS} = 63 ns
f_{QS} = 1.26 MHz
τ_{QS} = 49 ns
f_{QS} = 1.61 MHz
(f)
(g) T_{OC} = 50%
Pump = 352 mW
Pump = 879 mW
Pump = 1500 mW
(h)
τ_{QS} = 195 ns
f_{QS} = 0.89 MHz
τ_{QS} = 54 ns
f_{QS} = 1.99 MHz
τ_{QS} = 35 ns
f_{QS} = 2.51 MHz
(i)

Table 1 Summary of representative output characteristics of the laser under CW and Q-switched operation

	CW			Q-switching				
T_{OC}	P_{max} [mW] (η)	λ_0 [nm]	λ_{FWHM} [nm]	P_{max} [mW] (η)	λ_0 [nm]	λ_{FWHM} [nm]	f_{OS} [MHz]	τ_{OS} [ns]
1%	37 (2.8%)	1025.5	0.6	22 (1.8%)	1035.0	1.0	0.33–1.22	480–72
10%	265 (20.6%)	1035.3	0.6	187 (14.6%)	1035.1	0.8	0.84–1.61	111–49
50%	623 (51.3%)	1034.4	0.7	478 (39.8%)	1035.2	0.8	0.89–2.51	195–35

5 Conclusion

In summary, we have demonstrated passively Q-switched operation of a fs-DLW Yb:LuGG WG laser using SWCNTs as the SA. Comprehensive CW characterization across sequential cavity configurations confirmed excellent performance, with a maximum output power of 678 mW and a slope efficiency of 53.6% with a 70% OC. Single-transverse-mode operation was also verified. The WG propagation loss was estimated via Caird analysis to be 0.64 ± 0.07 dB/cm, indicating high fabrication quality. Stable Q-switched pulse trains were sustained for several hours by simply attaching SWCNT-coated OCs and an HR mirror to the WG facets. Q-switched performance was evaluated for T_{OC} of 1%, 10%, and 50% with detailed analysis of the temporal and frequency characteristics as a function of incident pump power. Among the investigated configurations, the best performance was obtained with 50% OC, yielding a maximum output power of 478 mW and a slope efficiency of 39.8%, along with a pulse duration of 35 ns at a repetition rate of 2.51 MHz. These results highlight the strong potential of fs-DLW Yb:LuGG WG lasers as compact, robust, and efficient pulsed laser sources. Furthermore, we expect that mode-locked operation at GHz-level repetition rates could be realized by employing smaller-core WGs, increased pump power, and appropriate dispersion management.

Author contributions Deok Woo Kim: Writing—review & editing, Writing—original draft, Visualization, Validation, Investigation, Formal analysis, Conceptualization. Seong-Eun Lim: Writing—review & editing, Resources. Ji-Hoon Park: Writing—review & editing, Resources. Xavier Mateos: Writing—review & editing, Validation, Resources. Weidong Chen: Writing—review & editing, Validation, Resources. Carolina Romero: Writing—review & editing, Resources. Javier Rodríguez Vázquez de Aldana: Writing—review & editing, Resources. Fabian Rotermund: Writing—review & editing, Validation, Investigation, Formal analysis, Supervision, Project administration, Methodology, Funding acquisition, Conceptualization.

Funding Open Access funding enabled and organized by KAIST. This work was supported by the National Research Foundation of Korea (NRF) (RS-2023-00208484, RS-2024-00408271), the Korea Institute of Energy Technology Evaluation and Planning (KETEP) (20224B10100040), and the Projects PID2022-141499OB-100 and PID2023-149836NB funded by MICIU/AEI/https://doi.org/10.13039/501100011033/ and by FEDER/UE. Department of Education of the Junta de Castilla y León and FEDER Funds is also gratefully acknowledged (Escalera de Excelencia CLU-2023-1-02).

Data availability No datasets were generated or analysed during the current study.

Declarations

Conflict of interest The authors declare that they have no known competing financial interests or personal relationships that could have appeared to influence the work reported in this paper.

References

1. H.R. Telle, G. Steinmeyer, A.E. Dunlop, J. Stenger, D.H. Sutter, U. Keller, Appl. Phys. B **69**, 327 (1999)
2. X. Yan, Q. Liu, X. Fu, H. Chen, M. Gong, D. Wang, Opt. Express **17**, 21956 (2009)
3. A. Yasukevich, N. Kondratyuk, N. Kuleshov, Quantum Electron. **39**, 1018 (2009)
4. W. Shi, S. Kerr, I. Utkin, J. Ranasinghesagara, L. Pan, Y. Godwal, R.J. Zemp, R. Fedosejevs, Optical resolution photoacoustic microscopy using novel high-repetition-rate passively Q-switched microchip and fiber lasers. J. Biomed. Opt. **15**(5), 056017 (2010). https://doi.org/10.1117/1.3502661
5. L. Gang, S. Hong-bin, L. Li, Z. Chu, M. Shao-juan, W. Yuan-bo, Laser-induced damages to charge coupled device detector using a high-repetition-rate and high-peak-power laser. Opt. Laser Technol. **47**, 221–227 (2013). https://doi.org/10.1016/j.optlastec.2012.07.030
6. B. Resan, R. Aviles-Espinosa, S. Kurmulis, J. Licea-Rodriguez, F. Brunner, A. Rohrbacher, D. Artigas, P. Loza-Alvarez, K.J. Weingarten, Opt. Express **22**, 16456 (2014)
7. S. Kawabata, S. Bai, K. Obata, G. Miyaji, K. Sugioka, Two-dimensional laser-induced periodic surface structures formed on crystalline silicon by GHz burst mode femtosecond laser pulses. Int. J. Extreme Manuf. **5**(1), 015004 (2023). https://doi.org/10.1088/2631-7990/acb133
8. T. Calmano, J. Siebenmorgen, O. Hellmig, K. Petermann, G. Huber, Appl. Phys. B **100**, 131 (2010)
9. J. Siebenmorgen, T. Calmano, K. Petermann, G. Huber, Opt. Express **18**, 16035 (2010)
10. S. Hakobyan, V.J. Wittwer, K. Hasse, C. Kränkel, T. Südmeyer, T. Calmano, Opt. Lett. **41**, 4715 (2016)

11. M.H. Kim, T. Calmano, S.Y. Choi, B.J. Lee, I.H. Baek, K.J. Ahn, D.-I. Yeom, C. Kränkel, F. Rotermund, Opt. Mater. Express **6**, 2468 (2016)
12. J.E. Bae, T.G. Park, E. Kifle, X. Mateos, M. Aguiló, F. Díaz, C. Romero, J. de Rodríguez Vázquez Aldana, H. Lee, F. Rotermund, Opt. Lett. **45**, 216 (2019)
13. J.E. Bae, S.Y. Choi, C. Kränkel, K. Hasse, F. Rotermund, Curr. Opt. Photon. **5**, 180 (2021)
14. T. Calmano, S. Müller, IEEE J. Sel. Top. Quantum Electron. **21**, 401 (2014)
15. F. Chen, J.V. de Aldana, Laser Photonics Rev. **8**, 251 (2014)
16. S. Chenais, F. Druon, F. Balembois, P. Georges, A. Brenier, G. Boulon, Opt. Mater. **22**, 99 (2003)
17. Y. Zhang, Z. Wei, B. Zhou, C. Xu, Y. Zou, D. Li, Z. Zhang, H. Zhang, J. Wang, H. Yu, Opt. Lett. **34**, 3316 (2009)
18. J. Liu, X. Tian, Z. Zhou, K. Wu, W. Han, H. Zhang, Opt. Lett. **37**, 2388 (2012)
19. K. Wu, L. Hao, H. Zhang, H. Yu, Y. Wang, J. Wang, X. Tian, Z. Zhou, J. Liu, R.I. Boughton, J. Opt. Soc. Am. B **29**, 2320 (2012)
20. J.M. Serres, P. Loiko, X. Mateos, H. Yu, H. Zhang, J. Liu, K. Yumashev, U. Griebner, V. Petrov, M. Aguilo, Opt. Quantum Electron. **48**, 1 (2016)
21. A. Diebold, Z. Jia, I.J. Graumann, Y. Yin, F. Emaury, C.J. Saraceno, X. Tao, U. Keller, Opt. Express **25**, 1452 (2017)
22. J. Dong, K.-I. Ueda, A.A. Kaminskii, Opt. Lett. **32**, 3266 (2007)
23. V. Petrov, M. Cinta Pujol, X. Mateos, O. Silvestre, S. Rivier, M. Aguilo, R.M. Solé, J. Liu, U. Griebner, F. Diaz, Laser Photonics Rev. **1**, 179 (2007)
24. K. Beil, S.T. Fredrich-Thornton, F. Tellkamp, R. Peters, C. Kränkel, K. Petermann, G. Huber, Opt. Express **18**, 20712 (2010)
25. L.D. DeLoach, S.A. Payne, L. Chase, L.K. Smith, W.L. Kway, W.F. Krupke, IEEE J. Quantum Electron. **29**, 1179 (2002)
26. R. Mary, G. Brown, S.J. Beecher, F. Torrisi, S. Milana, D. Popa, T. Hasan, Z. Sun, E. Lidorikis, S. Ohara, Opt. Express **21**, 7943 (2013)
27. Y. Ren, G. Brown, R. Mary, G. Demetriou, D. Popa, F. Torrisi, A.C. Ferrari, F. Chen, A.K. Kar, IEEE J. Sel. Top. Quantum Electron. **21**, 395 (2014)
28. Z. Yu, Y. Song, J. Tian, Z. Dou, H. Guoyu, K. Li, H. Li, X. Zhang, Opt. Express **22**, 11508 (2014)
29. X. Jiang, S. Gross, H. Zhang, Z. Guo, M.J. Withford, A. Fuerbach, Ann. Phys. **528**, 543 (2016)
30. X. Jiang, S. Gross, M.J. Withford, H. Zhang, D.-I. Yeom, F. Rotermund, A. Fuerbach, Opt. Mater. Express **8**, 3055 (2018)
31. J. Liu, F. Yang, J. Lu, S. Ye, H. Guo, H. Nie, J. Zhang, J. He, B. Zhang, Z. Ni, Nat. Commun. **13**, 3855 (2022)
32. W.B. Cho, J.E. Bae, S.C. Lee, N. Myoung, F. Rotermund, Curr. Opt. Photon. **7**, 738 (2023)
33. S. Yamashita, J. Light. Technol. **30**, 427 (2011)
34. J.W. Kim, S.Y. Choi, D.-I. Yeom, S. Aravazhi, M. Pollnau, U. Griebner, V. Petrov, F. Rotermund, Opt. Lett. **38**, 5090 (2013)
35. S.Y. Choi, T. Calmano, M.H. Kim, D.-I. Yeom, C. Kränkel, G. Huber, F. Rotermund, Opt. Express **23**, 7999 (2015)
36. S.Y. Choi, T. Calmano, F. Rotermund, C. Kränkel, Opt. Express **26**, 5140 (2018)
37. J.W. Kim, S.Y. Choi, J.E. Bae, M.H. Kim, Y.U. Jeong, E. Kifle, X. Mateos, M. Aguiló, F. Díaz, U. Griebner, Opt. Express **27**, 1488 (2019)
38. F. Rotermund, J. Korean Phys. Soc. **73**, 846 (2018)
39. D.L. Wood, K. Nassau, Appl. Opt. **29**, 3704 (1990)
40. J.A. Caird, S.A. Payne, P.R. Staver, A. Ramponi, L. Chase, IEEE J. Quantum Electron. **24**, 1077 (1988)
41. G. Spühler, R. Paschotta, R. Fluck, B. Braun, M. Moser, G. Zhang, E. Gini, U. Keller, J. Opt. Soc. Am. B **16**, 376 (1999)